Functional magnetic resonance microscopy at single-cell resolution in *Aplysia californica*

Guillaume Radecki[a], Romuald Nargeot[b,c], Ileana Ozana Jelescu[a], Denis Le Bihan[a], and Luisa Ciobanu[a,1]

[a]NeuroSpin, Commissariat à l'Energie Atomique et aux Energies Alternatives, 91191 Gif-sur-Yvette, France; and [b]Université de Bordeaux and [c]Centre National de la Recherche Scientifique, Institut de Neurosciences Cognitives et Intégratives d'Aquitaine, Unité Mixte de Recherche 5287, F-33000 Bordeaux, France

Edited by John G. Hildebrand, University of Arizona, Tucson, AZ, and approved May 8, 2014 (received for review March 4, 2014)

In this work, we show the feasibility of performing functional MRI studies with single-cell resolution. At ultrahigh magnetic field, manganese-enhanced magnetic resonance microscopy allows the identification of most motor neurons in the buccal network of *Aplysia* at low, nontoxic Mn^{2+} concentrations. We establish that Mn^{2+} accumulates intracellularly on injection into the living *Aplysia* and that its concentration increases when the animals are presented with a sensory stimulus. We also show that we can distinguish between neuronal activities elicited by different types of stimuli. This method opens up a new avenue into probing the functional organization and plasticity of neuronal networks involved in goal-directed behaviors with single-cell resolution.

neuroimaging | manganese-enhanced MRI

One of the current goals of neuroscience is to decipher the functional properties of the neuronal networks generating behaviors and their modulations by sensory stimuli. Studies on a variety of animal models have considerably advanced our understanding of the sensory control of automatic behaviors, including motor reflexes and rhythmic behaviors (locomotion and respiration) (1–4). In contrast, much less is known about the neuronal organization and adaptability of networks responsible for goal-directed actions. These complex behaviors, such as feeding or sexual activities, depend on the interaction between internally driven neuronal activity and external sensory inputs. Several macroscopic structures in the central nervous system (CNS) of vertebrates have been found to play a role in the organization of these behaviors (5). However, investigations of the cellular operations in these networks remain difficult because of their high degree of structural complexity.

Functional neuroimaging techniques have reached levels of performance that make possible the mapping of neural circuits (6). Among these techniques, MRI has been extensively applied to functional studies of mammalian brains. At present, the highest spatial resolution of such MRI experiments is of the order of $(0.3\ mm)^3$, averaging the signal from clusters of hundreds of neurons (7). Magnetic resonance (MR) microscopy (MRM) achieves higher resolution (of only a few micrometers) but requires long acquisition times, which prohibit its application to studying individual neurons in mammalian brains (8, 9). In the last decade, a new functional MR technique, manganese-enhanced MRI (MEMRI), has been successfully proven on various vertebrate animal models (10–12). MEMRI uses manganese, an MR contrast agent, to label active neurons. The amount of manganese that accumulates intracellularly is directly linked to neuronal activity, because the Mn^{2+} ion enters the neurons through calcium and nonspecific cationic channels (13–16). MEMRI was also applied to invertebrate animal models to visualize their nervous system and label activity-dependent Mn^{2+} uptake (17, 18).

In a previous study, we showed that MEMRI can be used to track axonal projections and follow changes in Mn^{2+} distribution induced by chemical stimulation in isolated neuronal preparations from *Aplysia californica* (19). The advantage of using this animal is that it has a simple nervous system composed of a relatively small number of neurons with large cell bodies, which can be resolved on high-resolution MR images.

In this manuscript, we introduce MEMRI as a functional imaging method that enables high-spatial resolution recordings of individual neurons of the buccal ganglia of *Aplysia*. We investigate neuronal responses to food-related stimuli (arousing and rewarding) and show that we can distinguish between different levels of neuronal activity that are generated spontaneously or in response to specific sensory stimuli. The method presented here can be extended to the entire nervous system of the animal, which will enable us to probe how different neuronal networks interact to generate motivated, goal-directed behaviors and how these behaviors are regulated by sensory inputs and learning.

Results

In Vivo Intraneuronal Accumulation of Mn^{2+}. Previously, we have shown the feasibility of performing MEMRI studies on isolated, functional *Aplysia* neuronal networks at low, nontoxic Mn^{2+} concentrations (19). In this work, we further designed a method to probe the neuronal activation elicited by peripheral sensory stimuli in the living *Aplysia* (Fig. 1*A*). In a first set of control experiments, we tested whether Mn^{2+} accumulates intracellularly on injection of $MnCl_2$ solution into the hemolymph of living animals. Two days before the experiments, the animals ($n = 10$) were isolated and food-deprived. After the $MnCl_2$ injection, they were allowed to behave normally for 45 or 90 min in an aquarium filled with artificial sea water (ASW) containing no food stimulus. Subsequently, they were anesthetized, and their bilateral buccal ganglia were resected (Fig. 1*B*). Each pair of ganglia was placed in a capillary containing ASW for imaging. MR imaging was performed at ultrahigh magnetic field, 17.2 T, using dedicated radio frequency solenoidal transceivers wrapped around

Significance

The direct observation with MRI of neuronal activity at single-neuron resolution represents a significant advancement in magnetic resonance (MR) microscopy and functional neuroimaging. The vast majority of high-resolution MR microscopy studies remain restricted to the generation of static images. This study shifts the focus of MR microscopy from noninvasive static imaging to dynamic investigations of activity in single cells and neuronal networks. Although most functional neuroimaging investigations are limited to averaging the signal from clusters of hundreds of neurons, we show that we are able to record the activity coming from individual neurons and their responses to sensory stimuli.

Author contributions: R.N., D.L.B., and L.C. designed research; G.R., I.O.J., and L.C. performed research; G.R., R.N., and L.C. analyzed data; and R.N. and L.C. wrote the paper.

The authors declare no conflict of interest.

This article is a PNAS Direct Submission.

Freely available online through the PNAS open access option.

[1]To whom correspondence should be addressed. E-mail: luisa.ciobanu@cea.fr.

This article contains supporting information online at www.pnas.org/lookup/suppl/doi:10.1073/pnas.1403739111/-/DCSupplemental.

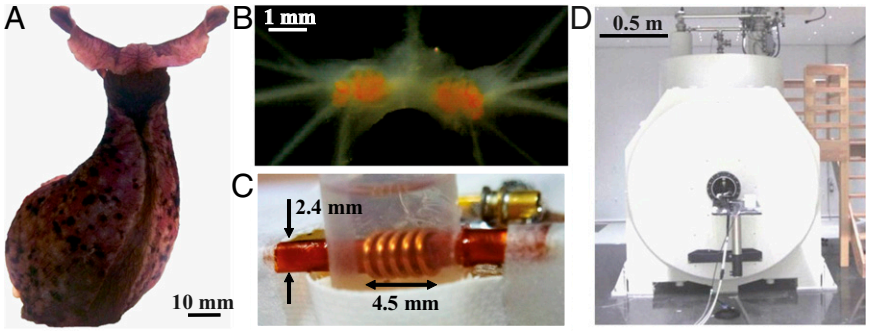

Fig. 1. Functional MRI of *A. californica*. Photographs of (*A*) *A. californica* in the feeding posture, (*B*) the caudal view of the isolated buccal ganglia, (*C*) the radiofrequency transceiver used for imaging, and (*D*) the 17.2 T MR imaging system.

the capillary containing the ganglia (Fig. 1 *C* and *D*). The acquisition protocol was optimized to detect the presence of manganese (19). Manganese accumulation within the ganglia produced hyperintense regions on T1-weighted images, because Mn^{2+} shortens the T1 relaxation time of the protons located in its vicinity. The comparison of these T1-weighted images (Fig. 2*A*) with the T2-weighted images (Fig. 2*B*) of the same ganglia showed that the hyperintense regions corresponded to somas of the buccal motor neurons, which can be individually identified on the basis of their size and relative position in the ganglia (20, 21). Thus, in freely behaving animals, the Mn^{2+} ions crossed some plasma membrane channels and accumulated into neurons. All the identified motor neurons in the buccal ganglia were found to contain Mn^{2+}, which is seen in the 3D rendering of the buccal ganglia shown in Movie S1. Between the two postinjection times at 45 and 90 min, we measured an average signal intensity increase of 9.5 ± 3.1%, reflecting an increase in the amount of Mn^{2+} accumulated intracellularly.

Stimulus-Evoked Neuronal Activation. A second set of experiments was designed to test whether the intracellular accumulation of Mn^{2+} in the buccal ganglia can be modified by the neuronal activity elicited by sensory stimuli. Twenty animals, food-deprived before $MnCl_2$ injection, were divided into two groups: nonstimulated (STIM0; $n = 10$) and stimulated (STIM1; $n = 10$). The nonstimulated *Aplysia* received no food stimulus postinjection, whereas the stimulated *Aplysia* were individually placed in an aquarium that contained *Ulva lactuca* and had unrestricted access to this food. Each of the two groups was divided into two subgroups of five animals each. The subgroups were different by the time interval, either 45 or 90 min, between the $MnCl_2$ solution injection and the anesthesia of the animal. After the anesthesia, the buccal ganglia of all the animals were isolated and imaged. Representative images of ganglia coming from stimulated animals are shown in Fig. 2*C*, T1-weighted, and Fig. 2*D*, T2-weighted. The average signal intensity measured in each identified neuron (as described in *Methods*) was found to be significantly higher in ganglia from stimulated than nonstimulated animals for both stimulation durations as confirmed by Kolmogorov–Smirnov (K-S) statistical comparison of the signal intensity distributions ($P < 4E\text{-}12$). The percent signal intensity changes accrued as a result of the two stimulation times are plotted in Fig. 3*A*. After calculating the average signal intensities in individual cells (*C*), the percent signal changes were calculated as $100 \times (I^{C,STIM1(45,90)} - I^{C,STIM0(45,90)})/I^{C,STIM0(45,90)}$, where $I^{C,STIM1}$ and $I^{C,STIM0}$ are signal intensities measured in ganglia coming from stimulated and nonstimulated animals, respectively; the indices 45 and 90 represent the stimulation duration in minutes. The data indicated that the percent signal change found after 45 min of stimulation is only marginally lower than that measured after 90 min of stimulation (Fig. 3*A*). The difference between the two stimulation times was 5%, on average, over all 14 identified cells. These results are in agreement with previous reports showing that exposure to food stimuli soon elicits a state of food-induced arousal and food consumption, which can last tenths of minutes and is associated with an increase in the neuronal excitability in several ganglia, including the buccal ganglia (7, 22). However, prolonged stimulation leads to a gradual decrease in these behavioral and neuronal responses as a result of satiation, sensory adaptation, and habituation (23–25).

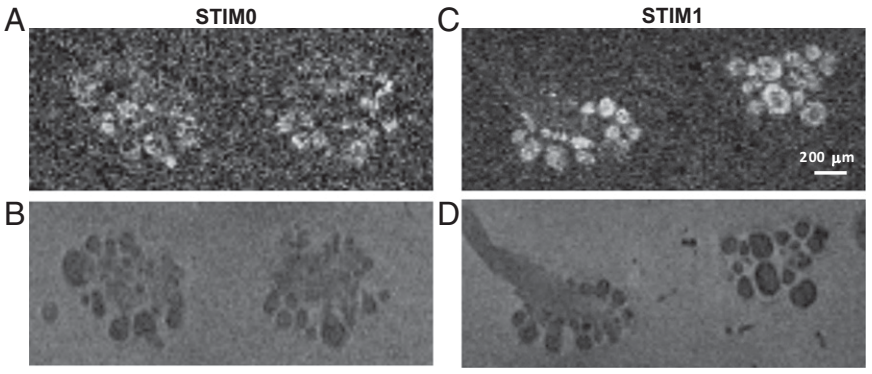

Fig. 2. Mn^{2+} accumulates intracellularly when injected into the living *Aplysia*. Representative MR images of ganglia from nonstimulated (STIM0; 90 min) and stimulated (STIM1; 90 min) animals. (*A* and *C*) Selected slices from T1-weighted images showing intracellular Mn^{2+} accumulation. The hyperintense regions represent individual neurons that have been identified using the T2-weighted images shown in *B* and *D*. In the T2-weigthed images, the neurons' somas can be easily distinguished, even in the absence of manganese. Spatial resolution: 25 μm isotropic. (Scale bar: 200 μm.)

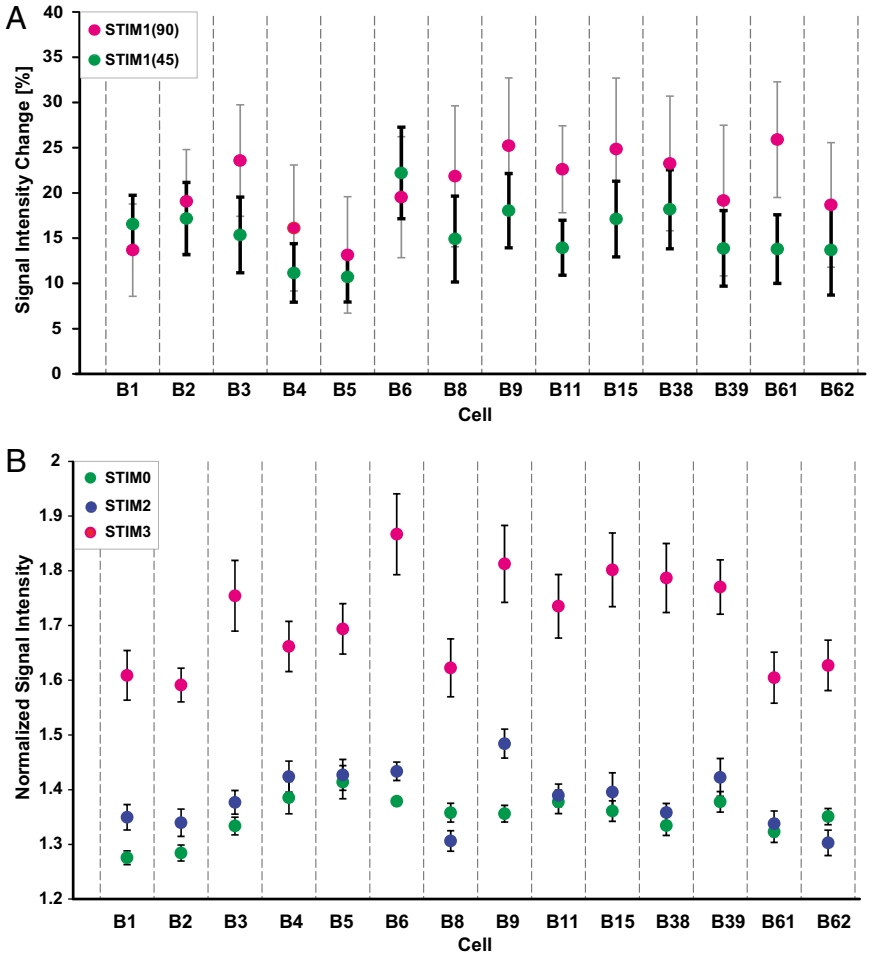

Fig. 3. The amount of Mn^{2+} accumulated inside neurons is stimulus-dependent. (*A*) Percent signal intensity change in STIM1 relative to STIM0 condition [defined as: $100\times(I^{C,STIM1(45,90)}-I^{C,STIM0(45,90)})/I^{C,STIM0(45,90)}$] for two different stimulus durations: 45 min in green and 90 min in magenta. (*B*) Average normalized signal intensity for three stimulation conditions: STIM0 (green; no food stimulus), STIM2 (blue; food-aroused and unfed animals), and STIM3 (magenta; food aroused and fed animals). $n = 10$ for each data point. The error bars represent the SEM.

Differential Neuronal Responses Revealed by MEMRI. There are at least two classes of food stimuli that modify the feeding behavior of *Aplysia* (23). The first class consists of external chemical and mechanical stimuli on the perioral zone that trigger the appetitive phase of the behavior, characterized by a state of food-induced arousal. The second class contains the internal chemical and mechanical stimuli in the buccal cavity that provide rewarding or punishing information, modifying the consummatory phase of the feeding behavior (26–28). Our next aim was to establish if MEMRI can be used to differentiate the neuronal activation resulting from these different stimuli. Fifteen Mn^{2+}-injected animals were divided into three groups according to the types of stimuli received. In the first group, the animals received no stimulation (STIM0; $n = 5$). In the second group, they received an arousing stimulus consisting of a piece of food (*U. lactuca*) maintained on the animals' perioral zone (STIM2; $n = 5$). Care was taken to prevent this stimulus from being bitten and ingested. In the third group, the animals received the same arousing stimulus, but they were allowed to bite and ingest it to provide internal rewarding stimuli (STIM3; $n = 5$). These conditions were maintained for 45 min before the isolation of the buccal ganglia. MEMRI responses were quantified for 14 individual neurons. Fig. 3*B* shows the signal intensity measured in these neurons for the three groups. As seen in Fig. 3*B*, the response of each individual neuron from the animals that were allowed to ingest food (STIM3) differed significantly from the response of the same neuron in the nonstimulated animals (STIM0). This difference was confirmed by K-S statistical comparison of the signal intensity distributions within neurons in STIM3 vs. STIM0 conditions ($P < 1E\text{-}17$ for all 14 neuron pairs). Thus, the activity of the motor neurons in the buccal ganglia was strongly modified by the arousing and rewarding stimuli applied together. The arousing stimulus alone had a less pronounced effect on the buccal motor activity; the difference in the signal intensity between the aroused but unfed (STIM2) and nonstimulated (STIM0) animals was small. However, for several neurons, we did observe (Table 1) significant differences between these two conditions. Specifically, the signal intensities were significantly increased in neurons B1, B2, B3, B6, and B9 and significantly decreased in neurons B8 under the STIM2 condition. Graphical representations of the signal intensity distributions under STIM0 and STIM2 are shown in Fig. 4 as typical examples of each type of neuronal response. The comparison of the neuronal responses between the aroused but unfed (STIM2) and the aroused and fed animals (STIM3) indicated that the signal intensity was significantly higher in STIM3 than STIM2 for all neurons ($P < 1E\text{-}25$). These results indicate that the modification in the buccal motor activity is essentially induced by stimuli from food intake and consumption rather than the arousing stimuli. Thus, MEMRI not only revealed changes in the neuronal properties that are

Table 1. Statistical comparison of the signal intensity distributions between STIM2 and STIM0 conditions

Cell	K-S *P* value	Motor function*
B9	9.5E-35[†]	Jaw closure
B1	7.3E-22[†]	Gut peristalsis
B2	8.4E-15[†]	Gut peristalsis
B3	4.8E-11[†]	Jaw closure
B6	5.7E-08[†]	Jaw closure
B8[‡]	8.8E-07[†]	Radula closure and retraction
B39	0.0016	Jaw closure
B4	0.0069	Undefined
B11	0.0221	Radula backward rotation
B62	0.0563	Radula protraction
B38	0.0582	Anterior jaw closure
B15	0.1392	Radula backward rotation and closure
B5	0.6277	Undefined
B61	0.8434	Radula protraction

*According to Church and Lloyd (20, 21) and Hurwitz et al. (37).
[†]$P < 0.001$.
[‡]The average signal intensity is lower for STIM2 condition.

induced by sensory stimuli in vivo, but also, it distinguished between different neuronal responses elicited by specific stimuli.

Quantification of the Intracellular Mn^{2+} Concentration and Assessment of Toxicity. The change in the amount of Mn^{2+} accumulated intracellularly because of sensory stimuli is clearly visible as a change in the measured longitudinal (T1) relaxation time (Fig. 5). Based on the measured T1s, we computed the intracellular Mn^{2+} concentration in several large neurons: B1, B2, B3, and B4 (Table 2). As seen in Table 2, the intracellular Mn^{2+} concentration in individual neurons varied depending on the sensory stimulation. Moreover, in all conditions and all identified neurons, the Mn^{2+} concentrations measured were under 100 μM, which is well below the value of 250 μM that was previously shown to not affect the neuronal electrical properties in the buccal ganglia of *Aplysia* (19) and much lower than concentrations locally injected in rodent studies (>5 mM) (29). In addition, we did not observe any change in animals' feeding behavior on $MnCl_2$ injection and therefore, expect no deleterious effects on the cellular and network properties that drive this behavior.

Discussion

This study shows that functional MRI can be used to image sensory-induced changes in neuronal activity at single-cell resolution. First, we have established that Mn^{2+} accumulates intracellularly when injected into the living *Aplysia*. Second, we found that the intracellular Mn^{2+} concentration in identified neurons changes in response to sensory stimuli. Third, we showed that the method implemented here can be used to distinguish different activities in an identified neuron in response to different sensory stimuli.

It has been previously shown that Mn^{2+} crosses the plasma membrane through voltage-gated calcium or nonspecific cationic channels (13, 14, 16). Consequently, the neuronal depolarization and opening of the ionic channels contribute to intracellular accumulation of Mn^{2+}. As a result, the Mn^{2+} concentration in neurons is expected to be related to the intensity and the duration of the neuronal activity. This study shows that the Mn^{2+} concentration measured in the buccal ganglia varied when the level of activity was changed by different food stimulation paradigms. In the absence of food, *Aplysia* generates a food-seeking behavior, during which the animal spontaneously emits repeated cycles of buccal movements. These movement cycles have a low frequency and are generated by the buccal motor pattern generating network in the buccal ganglia (30). This low spontaneous activity is expected to lead to a low Mn^{2+} concentration in the buccal ganglia coming from nonstimulated animals, which is what was measured with MRI. Conversely, food intake and swallowing provide various sensory stimuli on the inner surface of the buccal mass that reinforce the frequency and strength of the buccal movement cycles generated by the ganglia (25, 27, 28). These data agreed well with the strong increase in the Mn^{2+} concentration measured in the buccal ganglia coming from animals that were allowed to ingest food (STIM1 or STIM3). Moreover, the presence of food in the animal's surrounding environment, in contrast to its presence in the buccal cavity, stimulates the perioral zone (lips and rhinophores) and generates an appetitive behavior that does not require neuronal activity in the buccal ganglia (7, 23). The stimuli from this perioral zone are conveyed by peripheral nerves to the cerebral ganglion, which triggers activity in neuronal networks that are primarily located in the pedal-pleural ganglia rather than the buccal ganglia. Thus, the weak changes in the Mn^{2+} concentration in the buccal ganglia from aroused but unfed animals (STIM2) are consistent with a partial effect of the sensory stimuli from the perioral zone on the neuronal network in the buccal ganglia. Therefore, our results indicate that the functional MRI technique developed in this study can be successfully used to probe the different levels of neuronal activity that are generated spontaneously or in response to different sensory stimuli in a neuronal network.

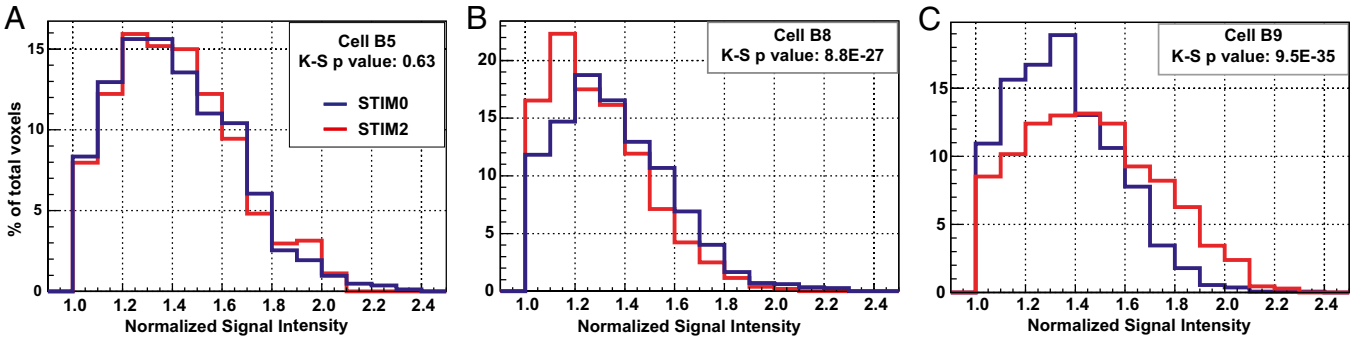

Fig. 4. MEMRI can distinguish different neuronal responses to a sensory stimulus. Distributions of voxel signal intensities (percentage of all voxels) obtained for neurons (*A*) B5, (*B*) B8, and (*C*) B9 for STIM0 (blue line) and STIM2 (red line). There is no statistically significant difference between the two stimulation conditions for neuron B5. For neurons B8 and B9, the distributions corresponding to STIM0 and STIM2 are statistically different. For neuron B8, the histogram corresponding to STIM2 is shifted to the left compared with STIM0, because it contains more voxels with lower signal intensity, suggesting a decrease in neuronal activity. For neuron B9, the situation is reversed, indicating that neuronal activity increases in the STIM2 vs. STIM0 condition. The data are binned in histograms for visualization purposes, and the K-S tests were performed on unbinned data.

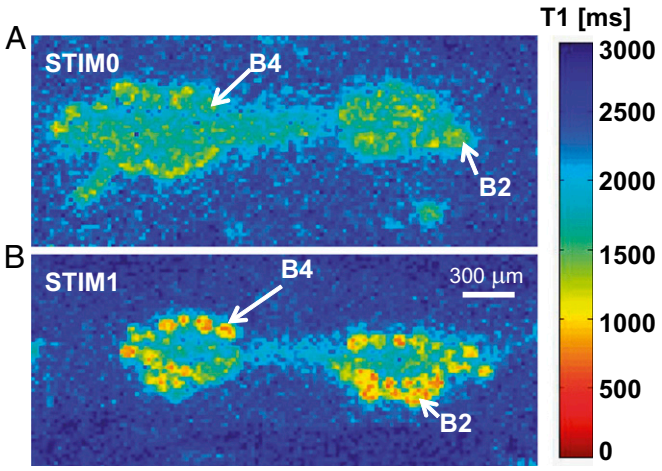

Fig. 5. The concentration of intracellularly accumulated Mn^{2+} can be measured in individual neurons. T1 maps of buccal ganglia coming from (*A*) a nonstimulated animal (STIM0) and (*B*) a food-aroused and fed animal (STIM3). Shorter T1 values indicate higher concentrations of Mn^{2+} corresponding to a higher level of neuronal activity. (Scale bar: 300 μm.)

The method implemented here also distinguishes different neuronal responses to the stimulation paradigms. In addition to the increase in the Mn^{2+} concentration as observed in most of the cells, a decrease in this concentration was also revealed in specific neurons for a particular stimulus (e.g., neurons B8 in STIM2 vs. STIM0). Although the significance of such a decrease in stimulated compared with nonstimulated animals is unclear, it is reasonable to trace it to a decrease or an inhibition of the spontaneous electrical activity of these neurons. Similarly, although it is difficult to clearly establish a link between the Mn^{2+} concentration and the motor function of specific motor neurons, our data suggest that this possibility must be more carefully investigated; in animals that were allowed to ingest food (STIM3), the signal intensity was higher in the retractor motoneuronal group (B3, B6, B9, B11, and B39) than the protractor motoneuronal group (B61 and B62). Such a result is consistent with the short and weak protraction phase followed by the long and powerful retraction phase of the radula that mediates food ingestion (31).

There are several ways to expand this method in the future. Although we have focused on the buccal ganglia in this study, there are other types of networks worth exploring, such as the cerebral ganglion, which is responsible for overall control and coordination of behavior, or the pedal-pleural ganglia, which mediate locomotion and head-weaving behavior. On a technical side, integrating multiple radio frequency (RF) detectors within one probe body (32) will expand our ability to simultaneously image several ganglia and will allow the investigation of the relationships between different networks, such as, for example, buccal and cerebral. Also, we envision using electrophysiological methods in vitro to stimulate identified sensory nerves or neurons in isolated ganglia to better quantify the relationship between the neuronal responses and MEMRI measurements.

Using the approach described in this work to investigate vertebrate nervous systems is challenging but certainly not impossible. MRM images of fixed human and porcine neurons have already been reported (33). It is conceivable that improved hardware technology (smaller microcoils and stronger magnetic field gradients) will significantly boost both the spatial and temporal resolutions, allowing single-cell functional MRM studies of live mammalian neuronal tissues.

Methods

Experimental Protocol. In these experiments, we used a total of 30 *A. californica* (Fig. 1*A*) purchased from National Resource for *Aplysia*. The animals were stored in two 200-L tanks of aerated and filtered ASW (Instant Ocean), and they were stimulated and fed with fresh algae *U. lactuca* (Station Biologique, Roscoff, France). Two days before the experiments, the animals were isolated and food-deprived. The day of the experiment, they were injected with $MnCl_2$ solution (100 mM $MnCl_2$, 345 mM NaCl, 10 mM KCl, 25 mM $MgCl_2$, 10 mM Hepes, pH 7.5; 500 μL/100 g). Based on the stimulation protocol performed during the postinjection period, the animals were divided into four groups.

STIM0: No stimulation (n = 10 animals). Animals were allowed to freely move in the tank in the absence of any food-related stimulus for 45 (five animals) or 90 min (five animals).

STIM1: Stimulation (n = 10 animals). Animals were left in the aquarium and had unrestricted access to food for 45 (five animals) or 90 min (five animals).

STIM2: Controlled stimulation without ingestion (n = 5 animals). Animals were stimulated for 45 min by a continuous application of food (*U. lactuca*) to the lips. Care was taken by the experimenter to avoid the biting or ingestion of the stimulus by the animals. This arousing stimulus triggers the appetitive behavior characterized by feeding posture, head-waving, and buccal movements.

STIM3: Controlled stimulation with ingestion (n = 5 animals). Food was presented for 45 min to the animals using the same procedure as for STIM2, but the animals were allowed to bite and ingest. This arousing and rewarding stimulus triggers the appetitive behavior (see above) and reinforces the consummatory behavior characterized by frequent repetitions of the ingestion movement cycles of the radula (a tongue-like organ), which drive food into the buccal cavity and gut.

Neuronal Preparation. The animals were anesthetized by injection of an isotonic magnesium chloride solution (360 mM $MgCl_2$, 10 mM Hepes, pH 7.5). The bilateral buccal ganglia (Fig. 1*B*) were resected and placed in a 2.5-mm OD glass capillary (VitroCom) filled with ASW (450 mM NaCl, 10 mM KCl, 30 mM $MgCl_2$, 20 mM $MgSO_4$, 10 mM $CaCl_2$, 10 mM Hepes, pH 7.5). All chemicals were from Sigma-Aldrich.

MRI Acquisitions. All MR acquisitions were performed on a 17.2 T Bruker imaging system (Bruker Biospin) (Fig. 1*D*) using a homemade solenoid (coil diameter = 2.6 mm, wire diameter = 0.7 mm) as an RF transceiver. The coil was immersed in FC-40 (3M) for improved B_0 homogeneity (Fig. 1*C*). Three different acquisitions were realized on each pair of ganglia. For T1 contrast we performed a 3D fast low angle shot (FLASH) acquisition with the following parameters: repetition time (TR) = 150 ms, echo time (TE) = 2.44 ms, acquisition time (TA) = 1 h, 25 μm isotropic resolution. Subsequently, we acquired 3D rapid acquisition with relaxation enhancement (RARE) data (TR = 3,200 ms, TE = 20 ms, TA = 2 h, 25 μm isotropic resolution) for T2 contrast, and 3D inversion recovery (IR) fast imaging with steady-state precession (FISP) data (TR = 8.4 ms, TE = 4 ms, n_{seg} = 6, TA = 1 h, resolution 30 × 30 × 100 μm, flip angle = 5°) with 20 inversion times (from 0 to 4,000 ms) for T1 mapping. The field of view was 2.2 × 2.2 × 5 mm^3 for all acquisitions. The cell bodies displayed a natural T2 contrast with respect to ASW, making them all visible on T2-weighted images, whereas the T1-weighted images revealed regions of Mn^{2+} uptake only.

Table 2. Intracellular Mn^{2+} concentrations for three different stimulation conditions

	Intracellular Mn^{2+} concentration (μM)		
Cell	STIM0	STIM2	STIM3
B1	18.3 ± 7.7	30.1 ± 16.6*	53.1 ± 22.1
B2	17.6 ± 7.0	29.0 ± 10.6*	51.6 ± 16.5
B3	22.6 ± 9.0	26.1 ± 8.8	84.1 ± 29.3
B4	26.3 ± 10.0	31.6 ± 12.1	64.4 ± 26.1

The errors represent SEM (n = 10).
*Nine cells were used for this average (one cell could not be identified).

NEUROSCIENCE

Data Processing. The acquired data were processed using Matlab (MathWorks); 3D renderings were produced using Amira software (Amira 5.3.3; TGS). Most of the large neurons in the buccal ganglia were identified on the T2-weighted images based on their relative position and size as described by Church and Lloyd (20, 21) [additional information in the work by Jelescu et al. (19)]. To correct for possible RF inhomogeneities, the signal intensity for each T1-weighted dataset was normalized to the signal of ASW. That is, in each slice in the 3D dataset, for a given voxel j at a particular position x along the solenoid axis, the signal intensity was normalized to the average ASW signal at the same position: $I_j = S_j / \overline{S^{ASW}}$ (Fig. S1). Regions of interest (ROIs) encompassing the identified neurons were manually traced on the T2-weighted images. The T1-weighted images were then coregistered with the T2-weighted images, and the voxel intensities within the defined ROIs were sorted by cell name for each ganglia. For each cell C, we calculated its signal intensity I^C as the average of I_j over all voxels j contained in the ROI of C. The analysis was limited to 14 cells, which were selected based on their ease of identification.

Statistical tests were performed using ROOT (34). All voxels corresponding to a particular cell and a particular stimulation condition were grouped together in distributions $\{I_j^{C,STIMk}\}$ (k = 0, 1, 2, 3), which therefore, incorporated both voxel-to-voxel and animal-to-animal intensity variations. For each ganglia pair, the cells located on the left and right sides were considered identical and grouped together. In our statistical treatment, the responses of cells to different stimulation conditions were compared by performing K-S tests to check whether the two sets of voxel intensities ($\{I_j^{C,STIMk}\}$ and $\{I_j^{C,STIMk'}\}$) are compatible with coming from the same distribution (35).

T_1 relaxation times were measured inside four large cells to minimize partial volume effects (cells B1, B2, B3, and B4 with average diameters of 160 μm). The mean IR FISP signal, averaged over manually drawn ROIs encompassing the soma of each cell, was plotted against inversion times. Using a least square fitting routine, we performed a three-parameter fit based on the following equation: $I(T_I) = I\ (1 - INV \exp(-T_I/T_1^*))$. In the equation, $INV = 1 + I_0/I_{stst}$, where I_0 is the signal at equilibrium, I_{stst} is the steady-state signal, T_I is the inversion time, and T_1^* is the apparent longitudinal relaxation time (36). Absolute T_1 was found using the relationship $T_1 = T_1^*\ (INV - 1)\ \cos(\alpha/2)$, where α is the flip angle of the FISP acquisition. Based on $[Mn^{2+}] = 1/r_1(1/T_1 - 1/T_1^0)$, these T_1 measurements gave access to the intracellular Mn^{2+} concentration, where T_1^0 = 1,740 ms is the relaxation time in control cells (from animals not injected with $MnCl_2$ solution), and $r_1 = 5.110^{-3}\ mM^{-1}ms^{-1}$ is the longitudinal relaxivity of Mn^{2+}, both measured at 17.2 T (19).

ACKNOWLEDGMENTS. The authors thank Boucif Djemaï and Jérémy Bernard for technical support. L.C. thanks Dr. C. I. Ciobanu for advice regarding the statistical analysis. Financial support was obtained through Grants ANR-08-PCVI-0009-01 (project DESIRE) and ANR-13-BSV5-0014-01 (project ANImE).

1. Nusbaum MP, Beenhakker MP (2002) A small-systems approach to motor pattern generation. *Nature* 417(6886):343–350.
2. Marder E, Bucher D, Schulz DJ, Taylor AL (2005) Invertebrate central pattern generation moves along. *Curr Biol* 15(17):R685–R699.
3. Kandel ER (2001) The molecular biology of memory storage: A dialogue between genes and synapses. *Science* 294(5544):1030–1038.
4. Edwards DH, Heitler WJ, Krasne FB (1999) Fifty years of a command neuron: The neurobiology of escape behavior in the crayfish. *Trends Neurosci* 22(4):153–161.
5. Balleine BW, O'Doherty JP (2010) Human and rodent homologies in action control: Corticostriatal determinants of goal-directed and habitual action. *Neuropsychopharmacology* 35(1):48–69.
6. Pastrana E (2013) Focus on mapping the brain. *Nat Methods* 10(6):481.
7. Goloshevsky AG, Wu CW-H, Dodd SJ, Koretsky AP (2011) Mapping cortical representations of the rodent forepaw and hindpaw with BOLD fMRI reveals two spatial boundaries. *Neuroimage* 57(2):526–538.
8. Ciobanu L, Seeber DA, Pennington CH (2002) 3D MR microscopy with resolution 3.7 microm by 3.3 microm by 3.3 microm. *J Magn Reson* 158(1-2):178–182.
9. Ciobanu L, Webb AG, Pennington CH (2003) Magnetic resonance imaging of biological cells. *Prog Nucl Magn Reson Spectrosc* 42(3):69–93.
10. Silva AC, Lee JH, Aoki I, Koretsky AP (2004) Manganese-enhanced magnetic resonance imaging (MEMRI): Methodological and practical considerations. *NMR Biomed* 17(8): 532–543.
11. Pautler RG, Koretsky AP (2002) Tracing odor-induced activation in the olfactory bulbs of mice using manganese-enhanced magnetic resonance imaging. *Neuroimage* 16(2): 441–448.
12. Van der Linden A, Van Meir V, Tindemans I, Verhoye M, Balthazart J (2004) Applications of manganese-enhanced magnetic resonance imaging (MEMRI) to image brain plasticity in song birds. *NMR Biomed* 17(8):602–612.
13. Geiger JE, Hickey CM, Magoski NS (2009) Ca2+ entry through a non-selective cation channel in Aplysia bag cell neurons. *Neuroscience* 162(4):1023–1038.
14. Crossgrove JS, Yokel RA (2005) Manganese distribution across the blood-brain barrier. IV. Evidence for brain influx through store-operated calcium channels. *Neurotoxicology* 26(3):297–307.
15. Narita K, Kawasaki F, Kita H (1990) Mn and Mg influxes through Ca channels of motor nerve terminals are prevented by verapamil in frogs. *Brain Res* 510(2):289–295.
16. Nelson MT (1986) Interactions of divalent cations with single calcium channels from rat brain synaptosomes. *J Gen Physiol* 87(2):201–222.
17. Herberholz J, Mims CJ, Zhang X, Hu X, Edwards DH (2004) Anatomy of a live invertebrate revealed by manganese-enhanced Magnetic Resonance Imaging. *J Exp Biol* 207(Pt 26):4543–4550.
18. Herberholz J, et al. (2011) Non-invasive imaging of neuroanatomical structures and neural activation with high-resolution MRI. *Front Behav Neurosci* 5:16.
19. Jelescu IO, Nargeot R, Le Bihan D, Ciobanu L (2013) Highlighting manganese dynamics in the nervous system of Aplysia californica using MEMRI at ultra-high field. *Neuroimage* 76:264–271.
20. Church PJ, Lloyd PE (1994) Activity of multiple identified motor neurons recorded intracellularly during evoked feedinglike motor programs in Aplysia. *J Neurophysiol* 72(4):1794–1809.
21. Church PJ, Lloyd PE (1991) Expression of diverse neuropeptide cotransmitters by identified motor neurons in Aplysia. *J Neurosci* 11(3):618–625.
22. Rosen SC, Weiss KR, Goldstein RS, Kupfermann I (1989) The role of a modulatory neuron in feeding and satiation in Aplysia: Effects of lesioning of the serotonergic metacerebral cells. *J Neurosci* 9(5):1562–1578.
23. Kupfermann I (1974) Feeding behavior in Aplysia: A simple system for the study of motivation. *Behav Biol* 10(1):1–26.
24. Horn CC, Benjamin PR, Weiss KR, Kupfermann I (1999) Decrement of the response of a serotonergic modulatory neuron (the metacerebral cell) in Aplysia, during repeated presentation of appetitive (food) stimuli. *Neurosci Lett* 267(3):161–164.
25. Schwarz M, Susswein AJ (1986) Identification of the neural pathway for reinforcement of feeding when Aplysia learn that food is inedible. *J Neurosci* 6(5):1528–1536.
26. Susswein AJ, Schwarz M, Feldman E (1986) Learned changes of feeding behavior in Aplysia in response to edible and inedible foods. *J Neurosci* 6(5):1513–1527.
27. Brembs B, Lorenzetti FD, Reyes FD, Baxter DA, Byrne JH (2002) Operant reward learning in Aplysia: Neuronal correlates and mechanisms. *Science* 296(5573):1706–1709.
28. Nargeot R, Petrissans C, Simmers J (2007) Behavioral and in vitro correlates of compulsive-like food seeking induced by operant conditioning in Aplysia. *J Neurosci* 27(30):8059–8070.
29. Silva AC, Bock NA (2008) Manganese-enhanced MRI: An exceptional tool in translational neuroimaging. *Schizophr Bull* 34(4):595–604.
30. Nargeot R, Simmers J (2012) Functional organization and adaptability of a decision-making network in aplysia. *Front Neurosci* 6:113.
31. Morton DW, Chiel HJ (1993) In vivo buccal nerve activity that distinguishes ingestion from rejection can be used to predict behavioral transitions in Aplysia. *J Comp Physiol A Neuroethol Sens Neural Behav Physiol* 172(1):17–32.
32. Ciobanu L, Jayawickrama DA, Zhang X, Webb AG, Sweedler JV (2003) Measuring reaction kinetics by using multiple microcoil NMR spectroscopy. *Angew Chem Int Ed Engl* 42(38):4669–4672.
33. Flint JJ, et al. (2009) Magnetic resonance microscopy of mammalian neurons. *Neuroimage* 46(4):1037–1040.
34. Brun R, Rademakers F (1997) ROOT An object oriented data analysis framework. *Nucl Instrum Methods Phys Rev A* 389(1–2):81–86.
35. Eadie WT, Drijard D, James FE, Roos M, Sadoulet B (1972) *Statistical Methods in Experimental Physics* (American Elsevier Publishing Company, New York).
36. Schmitt P, et al. (2004) Inversion recovery TrueFISP: Quantification of T(1), T(2), and spin density. *Magn Reson Med* 51(4):661–667.
37. Hurwitz I, Neustadter D, Morton DW, Chiel HJ, Susswein AJ (1996) Activity patterns of the B31/B32 pattern initiators innervating the I2 muscle of the buccal mass during normal feeding movements in Aplysia californica. *J Neurophysiol* 75(4):1309–1326 (1996).